Inhalation Toxicology, 2009; 21(S1): 55–60

informa
healthcare

RESEARCH ARTICLE

Size dependence of the translocation of inhaled iridium and carbon nanoparticle aggregates from the lung of rats to the blood and secondary target organs

Wolfgang G. Kreyling[1,2,3], Manuela Semmler-Behnke[1,2,3], Jürgen Seitz[1,3], Wilfried Scymczak[1,2,4], Alexander Wenk[1,3], Paula Mayer[1,3], Shinji Takenaka[1,2,3], and Günter Oberdörster[5]

[1]Helmholtz Center Munich, [2]Focus Network Nanoparticles and Health, [3]Institute of Lung Biology and Disease, [4]Institute of Radiation Protection, Neuherberg/Munich, Germany, and [5]Department of Environmental Medicine, University of Rochester, Rochester, New York, USA

Abstract

Currently, translocation of inhaled insoluble nanoparticles (NP) across membranes like the air-blood barrier into secondary target organs (STOs) is debated. Of key interest are the involved biological mechanisms and NP parameters that determine the efficiency of translocation. We performed NP inhalation studies with rats to derive quantitative biodistribution data on the translocation of NP from lungs to blood circulation and STOs. The inhaled NP were chain aggregates (and agglomerates) of either iridium or carbon, with primary particle sizes of 2–4 nm (Ir) and 5–10 nm (C) and aggregate sizes (mean mobility diameters) between 20 and 80 nm. The carbon aggregates contained a small fraction (< 1%) of Ir primary particles. The insoluble aggregates were radiolabeled with ^{192}Ir. During 1 h of inhalation, rats were intubated and ventilated to avoid extrathoracic NP deposition and to optimize deep lung NP deposition. After 24 h, ^{192}Ir fractions in the range between 0.001 and 0.01 were found in liver, spleen, kidneys, heart, and brain, and an even higher fraction (between 0.01 and 0.05) in the remaining carcass consisting of soft tissue and bone. The fractions of ^{192}Ir carried with the carbon NP retained in STOs, the skeleton, and soft tissue were significantly lower than with NP made from pure Ir. Furthermore, there was significantly less translocation and accumulation with 80-nm than with 20-nm NP aggregates of Ir. These studies show that both NP characteristics—the material and the size of the chain-type aggregates—determine translocation and accumulation in STOs, skeleton, and soft tissue.

Keywords: *Aggregates; carbon nanoparticle; inhalation; iridium nanoparticle; rat lung; secondary target organs; translocation*

Introduction

With the advent of nanotechnology the interaction of nanoparticles (NP) with biological systems including mammalian organisms has become a very active area of basic and applied research. As NP are of the same size as typical cellular components and proteins, they are suspected to evade the natural defense system of the human organism, thus being capable of generating permanent cell damage (Donaldson et al., 2004). Although there is substantial evidence from recent toxicological studies that NP may cause adverse health effects (Oberdörster et al., 2005a, 2005b), the fundamental cause–effect relationships are not yet understood (Maynard et al., 2006). Therefore, the elementary processes of NP interaction with biological systems need to be investigated at macroscopic and microscopic levels (Kreyling et al. 2007). For an effect-based assessment, potential target organs and target cells need to be known (Borm & Kreyling, 2004). Target organs may not be restricted to the lung, the primary organ of intake, but may include secondary target organs (STOs). Hence, an important prerequisite of effect assessment is the determination of NP translocation to the blood circulation and the subsequent accumulation in

Address for Correspondence: Dr. Wolfgang G. Kreyling, Helmholtz Center Munich—German Research Center for Environmental Health, Institute of Lung Biology and Disease, Ingolstaedter Landstr. 1, 85764 Neuherberg/Munich, Germany. E-mail: kreyling@helmholtz-muenchen.de

(Received 26 March 2009; accepted 02 April 2009)

ISSN 0895-8378 print/ISSN 1091-7691 online © 2009 Informa UK Ltd
DOI: 10.1080/08958370902942517

STOs and target cells. To obtain a comprehensive overview on the quantitative level of NP biodistribution, an analysis is required taking into account NP retention in the entire organism as well as the excretion.

In this study we have explored the translocation characteristics of very small NP (≤ 10 nm) contained in much larger chain-type aggregates. Moreover, we have addressed the question of whether the efficiency of translocation depends on the NP material, here iridium and carbon. While iridium may be considered a somewhat exotic choice, it is ideally suited for these studies for two reasons: first, its insolubility, and second, the ability to conveniently generate radiolabeled isotopes. Chain-type aggregates of elemental carbon are highly relevant because (i) they are representing the core material of many ambient nanoparticles incidentally generated in various types of combustion, and (ii) carbon black NP are routinely used in a variety of technological applications.

Methods

Animals

Young, adult, healthy, male WKY/Kyo@Rj rats (Janvier, France; body weight 250 ± 20 g) were housed in an air-conditioned (55 ± 5% relative humidity) and temperature-controlled (22 ± 3°C) room. They were maintained on a 12-h day/night cycle. Rats were allowed to acclimate to the facility for a minimum of 7 days prior to use. Twelve rats were randomly assigned into three groups for the exposure to one of the three aerosols. The studies were conducted under federal guidelines for the use and care of laboratory animals and were approved by the "Regierung von Oberbayern" (District Government of Upper Bavaria, Approval-No.: 211-2531-108/99) and by the Institutional Animal Care and Use Committee of Helmholtz Center Munich.

Aerosol production and characterization

Aerosols of iridium and carbon nanoparticles radiolabeled with ^{192}Ir were generated with a spark generator (GFG 1000, Palas) (Roth et al., 2004). In case of the ^{192}Ir-labeled iridium nanoparticles, sparks of constant energy were ignited between 2 adjacent neutron-activated pure iridium electrodes at a frequency of either 3 or 150–180 Hz in an argon stream of 3.5 L/min to achieve the two NP sizes. In the case of the iridium-labeled carbon nanoparticles only one electrode consisted of radiolabeled iridium and the other was just a pure graphite rod. The radio isotope ^{192}Ir is a beta and gamma emitter with a half-life of 74 days and gamma energies of 296, 308, 316, 468, and 588 keV (26, 29, 73, 47, and 5% efficiency, respectively); there are also some higher and some lower energies of low efficiency. Gamma spectroscopy was performed using the photo peaks of 296, 308, and 316 keV. To achieve a sufficient ^{192}Ir radioactivity in the inhaled aerosol the miniaturized iridium electrodes (1 mm diameter; 4 mm length), neutron activation parameters were chosen to obtain a total of 5–7 GBq ^{192}Ir activity in both electrodes. At the exit of the spark generator the aerosol was quasi-neutralized by a radioactive ^{85}Kr source (40 MBq). The aerosol was diluted with nitrogen and—for rat exposures—with oxygen adjusted to obtain 20% oxygen and the synthetic air was conditioned at 50–60% relative humidity and 37°C for rat exposure as described earlier (Kreyling et al., 2002). Size distribution and number concentration were monitored continuously by a differential mobility particle sizer (DMPS; classifier model 3070 and CPC model 7610, TSI) and a condensation particle counter (CPC3022A, TSI), respectively. Lower particle size detection limit of the former was 10 nm. Connecting tubes were selected such that the aerosol residence time until analysis was the same as the residence time until rat exposure to assure precise measurements of the aerosol the rats were inhaling. ^{192}Ir radioactivity of the aerosol was determined by continuous aerosol sampling at a flow rate of 0.2 L/min, volume measurement, and gamma counting in a well-type scintillation detector. Aerosol mass concentration was derived from the given specific activity of the electrodes.

Inhalation

For inhalation, rats were ventilated during 1 h via an endotracheal tube. Anesthesia for the intubation and the ventilation procedure in the plethysmograph box was described earlier (Kreyling et al., 2002; Semmler et al., 2004).

NP clearance and biodistribution

After exposure the anesthesia of the rats was antagonized as described earlier (Kreyling et al., 2002; Semmler et al., 2004). During the next 24 h the rats were kept in metabolic cages and excreta were collected separately and quantitatively. After that time, rats were killed by exhaustive exsanguination after intraperitoneal anaesthesia as described previously (Kreyling et al., 2002). All organs, samples of muscle and bone, the entire skin, and the remaining carcass were taken. About 70% of the blood volume was sampled via the abdominal aorta estimating the blood volume from the body weight. Prior to autopsy a bronchoalveolar lavage (BAL) was performed applying 6 times 5 ml phosphate-buffered saline under gentle massage of the thorax. ^{192}Ir activity of lavaged cells and supernatant and the total and differential cell counts were determined. A complete balance of ^{192}Ir activity retained in all organs and tissues and in the entire body and clearance via excretion was measured gamma spectroscopically in 2 scintillation detectors equipped with either a 1-L well-type NaI(Tl) detector or a 20-cm^3 well-type detector (Kreyling et al., 2002).

Correction for NP fractions in rest blood volumes of selected organs was obtained based on data from an earlier report (Oeff and Konig, 1955). This publication reported not only blood volumes of each organ as a function of the body weight, but also the residual blood volume after thorough exsanguination by heart puncture very similar to our protocol. NP concentration in blood was determined from the measured blood activity and the sampled blood volume. With these data the NP fraction in the remaining blood volumes of each organ was estimated and subtracted from the

organ fraction in order to observe only the fraction of NP associated with the organ tissue.

Statistical analysis

For statistical data analysis Student's *t*-tests were performed using Microsoft EXCEL 2003 software. Statistical significance was considered when $p < .05$.

Results and discussion

Aerosol characterization

Besides two different sizes of ultrafine ^{192}Ir aerosols—count median diameter (CMD) between 15 and 20 nm and 70 to 80 nm—the composite iridium-labeled carbon NP of 22 to 25 nm size were produced with the spark generator. Particle size distributions and aerosol characteristics of the iridium NP aerosols were presented previously (Kreyling et al., 2002). In the following the three particles are termed either 20-nm or 80-nm iridium NP or 25-nm composite carbon iridium NP. The composite carbon iridium NP were slightly larger than the 20-nm iridium NP, but otherwise aerosol characteristics like concentration and geometric standard deviation of the size distribution were very similar. The transmission electron micrographs of all three NP clearly show non-isometric chain-aggregated and agglomerated particles (composite NP not shown; iridium NP micrographs in Kreyling et al., 2002). Aggregation of primary particles occurred in the hot zone right next to the surface of the iridium electrodes while these aggregates continued to agglomerate during cooling due to the high particle concentration—they are called chain aggregated NP in the following. The 80-nm iridium NP consisted of the same sized primary particles but were much more agglomerated due to higher primary particle concentration in the argon flow as a result of the higher spark frequency when compared to the 20-nm iridium NP. Chain aggregation of the freshly formed primary particles in the hot zone next to each of the electrodes is likely followed by agglomeration at lower temperatures

Using time-of-flight secondary ion mass spectroscopy (TOF-SIMS) and electron microscopy, intense studies were performed on the composition of the composite ^{192}Ir labeled iridium–carbon chain aggregate NP. Carbon and iridium were not found to be mixed in primary particles but the formation of primary carbon particles separates them from primary ^{192}Ir-labeled iridium particles (Szymczak et al., 2007). The TOF-SIMS analyses showed that the iridium NP were particularly oxidized at their surface. Primary iridium particles with a size of 2–4 nm or carbon particles of 5–10 nm size were estimated in transmission electron micrographs (data not shown). In fact, condensation of primary particles appears immediately upon evaporation from the surface of the electrodes, while coagulation (aggregation and agglomeration) of the primary particles occurs subsequently during cooling. According to the evaporation thermodynamics, during spark ignition on the surface of both electrodes > 95% of the chain aggregate mass consisted of the primary carbon NP and < 5% of the iridium NP; i.e., chain aggregates consisted of primary carbon NP with only very few ^{192}Ir-labeled iridium NP, as schematically shown in Figure 1. Hence, the obtained composite NP can be considered as carbon chain aggregates spiked with a few primary ^{192}Ir-labeled iridium NP.

According to the specific ^{192}Ir radioactivity (yielding a ^{192}Ir isotope to stable iridium atom ratio of $< 10^{-5}$) and the size of the primary iridium particles, statistically each primary particle does not contain more than one ^{192}Ir radio isotope.

Deposition

Due to endotracheal intubation there was neither extrathoracic particle deposition nor pelt contamination. Total deposition data of the 20- and 80-nm iridium NP relative to the inhaled aerosols were reported previously (Kreyling et al., 2002). Similar to the 20-nm Ir NP, the deposition of the composite iridium–carbon NP was also in the range of 1 μg per rat. In Table 1 the rapidly cleared fraction of the 20-nm Ir NP is 2.5-fold higher than that of 80-nm Ir NP, corresponding to the higher diffusion and, hence, increased deposited fraction in the airways when compared to 80-nm Ir NP.

Lung retention and fast clearance

Table 1 provides the retained NP fraction in the lungs after 24 h, as well as the lavageable NP fraction in BAL and the rapidly cleared fraction from the intrathoracic airways into the gastrointestinal (GI) tract and excreted feces. All fractions are relative to the initial NP deposit in the lungs.

Gut absorption and NP solubility

As previously shown in auxiliary studies, gut absorption of the rapildy cleared NP from the airways to the GI tract was negligible (Kreyling et al., 2002). In addition, in this previous

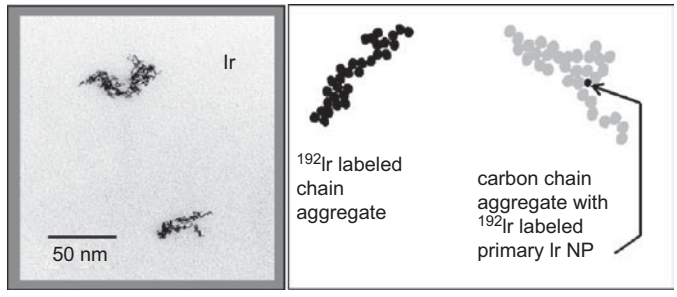

Figure 1. Left: TEM of iridium chain aggregates. Right: Schematic drawings of chain aggregates of only iridium primary particles (left) and of mostly carbon primary particles spiked with a single iridium primary particle.

Table 1. Fractions of retained or cleared NP relative to the initial NP deposit after 24 h.

NP	24-h Lung retention including BAL fraction	Rapidly cleared NP fraction	BAL fraction
Composite Ir–carbon NP, 25 nm	0.70 ± 0.07	0.23 ± 0.08	0.08 ± 0.07
Ir NP, 20 nm	0.64 ± 0.04	0.30 ± 0.05	0.12 ± 0.02
Ir NP 80 nm	0.86 ± 0.09	0.12 ± 0.08	0.17 ± 0.05

report, auxiliary studies of inhaled soluble Ir salt aerosols were used to determine the distribution pattern and to estimate iridium dissolution from the chain-aggregated NP. These showed negligible dissolution of the iridium NP consisting of the 2- to 5-nm primary particles. Hence, also the primary iridium particles within the composite iridium–carbon NP are insoluble because they are the same primary particles produced the same way.

Translocation

Figure 2 shows significantly lower accumulation of 80-nm iridium particles compared to the 20-nm particles in all STOs, blood, and remaining carcass; thereby it indicates the inverse size dependency of translocation from the lung epithelium to blood: All fractions of the 80-nm NP are about one order of magnitude lower than those of 20-nm NP. The rapidly cleared fraction in the GI tract and feces was excluded in this calculation. Note the rather high fractions of both NP circulating in blood 24 h after inhalation. Since NP fractions in the remaining blood volume after exsanguinations are likely to superimpose the NP fractions in the organs, the blood-associated fraction of each organ was estimated as described in the Methods section and the organ fractions were corrected. This is shown later, in Figure 4.

There are significant differences between accumulated fractions of the similar sized iridium NP and the composite carbon–iridium NP in the remaining carcass and in all STOs—except liver, shown in Figure 3. This finding shows the dependency of translocation and accumulation in STOs on different chain-aggregated NP materials—iridium NP versus carbon NP spiked with few iridium primary particles—of the same size. The very low composite NP fraction in blood indicates that these NP have short residence time in blood and are taken up rapidly by the liver such that the NP fraction in the liver is close to that for the iridium NP.

In Figures 2 and 3 there also are much higher NP accumulations in the remaining carcass made up of soft tissue mostly, as well as rest blood, skin, and skeleton, when compared to STOs. No published data are available for the rest blood in the remaining carcass. However, by the applied exhaustive method of exsanguination about 70% of the whole blood was collected. Subtracting 30% of the NP fraction in total blood reduces the NP fraction in the carcass only minimally. Hence, the NP fraction is mostly associated with soft tissue and bone.

In Figure 4, fractions of all three NP were corrected for NP contained in the rest blood of each organ after exsanguination—see the Methods section. Corrections are only detectable in blood-rich organs like the liver. Yet in this graph the differences among all three NP become clear. In all STOs and in total blood the 20-nm iridium NP fractions are significantly higher than those of the similar sized 25-nm composite NP and the larger 80-nm NP. Hence, both characteristics, the material and the size, of these chain-aggregated NP influence the translocation and accumulation in STOs. Even though the exposure was short and the deposited amount of rather inert NP was low, we cannot exclude vasoconstriction, as it is reported in the literature (Nemmar et al., 2002). However, if vasoconstriction occurs, the blood content in a single organ would be lower than we actually

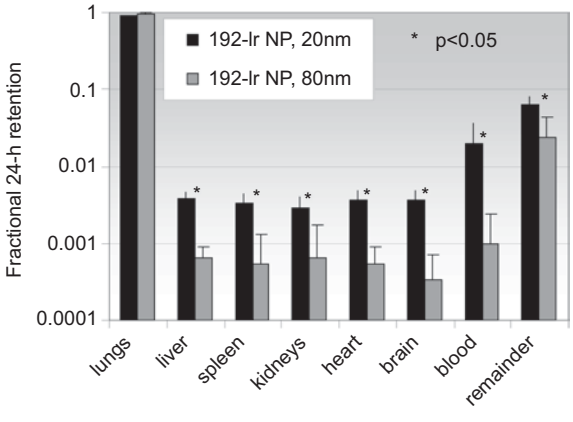

Figure 2. Twenty-four-hour retention of 20- and 80-nm iridium NP in various STOs, total blood, and the remaining carcass. Mean values (± STD) obtained from four rats in each group are shown. The rapidly cleared fraction in GI tract and feces was excluded from the denominator in this calculation.

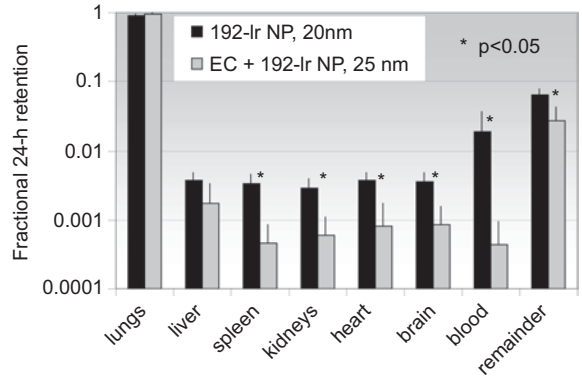

Figure 3. Twenty-four-hour retention of 20-nm iridium NP and 25-nm composite iridium– carbon NP (EC+^{192}Ir NP) in various STOs, total blood, and the remaining carcass. Mean values (± STD) obtained from four rats in each group are shown. The rapidly cleared fraction in GI tract and feces was excluded from the denominator in this calculation.

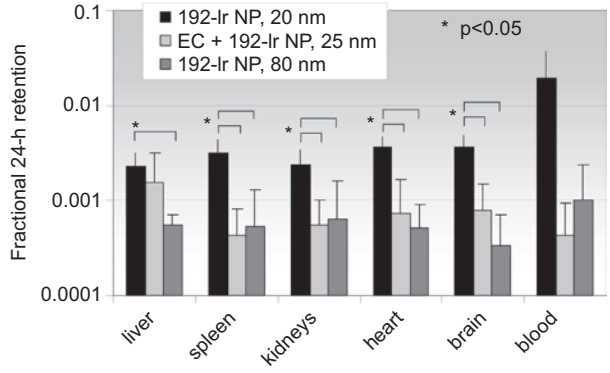

Figure 4. Twenty-four-hour retentions of all three NP in various STOs without the NP fractions associated with the rest blood in each organ after exsanguination. Mean values (± STD) obtained from four rats in each group are shown.

estimate; therefore, our correction represents a conservative estimate.

Figure 5 shows accumulated fractions of all three NP in the sum of all STOs, estimated skeleton, and soft tissue. The latter are based on the bone and muscle sample measurements. Also in the skeleton and soft tissue the significant differences in the material and the size of the three NP were observed. Even though the fractions in soft tissue appear to be highest, the NP concentrations are rather low because of the large mass fractions of soft tissue. Although this was not tested, we hypothesize that in the skeleton NP will be found in the bone marrow since the NP entered the skeleton via blood circulation. Our hypothesis is confirmed by recent studies using different NP (Rinderknecht et al. 2008). These findings suggest further investigations on adverse responses in bone marrow and blood during continuous NP exposure since the NP dose observed after a single 1-h exposure may accumulate during chronic exposure to inhaled NP.

The results presented here are in contrast to our earlier findings obtained from similar inhalation studies using 25-nm sized ^{13}C-labeled carbon NP (Oberdörster et al., 2002) showing a much larger NP fraction in the liver of rats after 24 h when compared to our data shown in Figures 2 and 3 for 20-nm sized iridium NP and 25-nm sized composite iridium–carbon NP, respectively. The use of the ^{192}Ir radiolabel in the new studies appears to be advantageous since there is no natural background of this radio-isotope in biological systems. In contrast, the previously stable isotope ^{13}C occurs abundantly in all biological samples at a level of about 1%; actually the ^{13}C:^{12}C ratio is very constant in biological samples but the total carbon content in organs and tissues undergoes some variability. Since the deposited ^{13}C dose of the inhaled carbon NP in the former study was only a small fraction (~10%) of the naturally occurring endogenous ^{13}C, the variability of the total carbon content may have affected the former results.

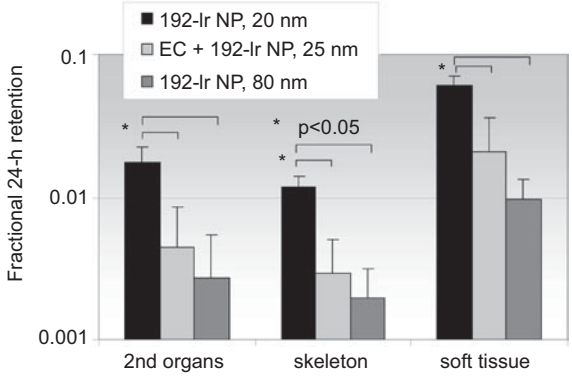

Figure 5. Twenty-four-hour retentions of all three NP in the sum of all STOs, with estimated bone and muscle fraction. The latter were calculated from the NP fraction determined in a bone and a muscle sample and assuming that 10% and 70% of the body weight is attributed to the skeleton and soft tissue. Mean values (± STD) obtained from four rats in each group are shown.

Since the iridium NP are not commonly found in the ambient environment, we compared those with environmentally relevant carbon NP radiolabeled with primary iridium particles. We chose sizes that are relevant in the ambient atmosphere, as the ambient particle number concentration is highest in the range of 10–30 nm (Kreyling et al., 2003) and the diesel particle volume concentration in ambient air peaks at about 100 nm (Kittelson, 1998).

Conclusion

Administering the aerosol via an endotracheal tube was advantageous since no NP deposited in extrathoracic airways and NP did not contaminate the pelt. One day after inhalation all three NP deposited on thoracic airways were cleared predominantly to the larynx into the GI tract and feces. All three NP were retained predominantly in the peripheral lungs. However, small fractions of all three NP were translocated across the lung epithelium into blood and accumulated in STOs and skeleton and soft tissue, such that after 24 h, fractions of all three NP were found in liver, spleen, kidneys, heart, brain, and skeleton and even higher fractions in soft tissue. These studies show that both NP characteristics—the material and the size of these chain-aggregated NP—determine the translocation and accumulation in STOs, skeleton, and soft tissue.

***Declaration of interest*:** This work was supported in part by EU FP6 PARTICLE_RISK 012912 (NEST) and by U.S. National Institutes of Health grant HL070542. The authors alone are responsible for the content and writing of the paper.

References

Borm PJ and Kreyling W. 2004. Toxicological hazards of inhaled nanoparticles—Potential implications for drug delivery. J Nanosci Nanotechnol 4:521–531.

Donaldson K, Stone V, Tran CL, Kreyling W, and Borm PJ. 2004. Nanotoxicology. Occup Environ Med 61:727–728.

Kittelson DB. 1998. Engines and nanoparticles: A review. J Aerosol Sci 29:575–588.

Kreyling WG, Semmler M, Erbe F, Mayer P, Takenaka S, Schulz H, Oberdörster G, and Ziesenis A. 2002. Translocation of ultrafine insoluble iridium particles from lung epithelium to extrapulmonary organs is size dependent but very low. J Toxicol Environ Health A 65:1513–1530.

Kreyling WG, Tuch T, Peters A, Pitz M, Heinrich J, Stolzel M, Cyrys J, Heyder J, and Wichmann HE. 2003. Diverging long-term trends in ambient urban particle mass and number concentrations associated with emission changes caused by the German unification. Atmos Environ 37:3841–3848.

Kreyling WG, Semmler-Behnke M, and Moeller W. 2006. Health implications of nanoparticles. J Nanoparticle Res 8:543–562.

Maynard AD, Aitken RJ, Butz T, Colvin V, Donaldson K, Oberdörster G, Philbert MA, Ryan J, Seaton A, Stone V, Tinkle SS, Tran L, Walker NJ, and Warheit DB. 2006. Safe handling of nanotechnology. Nature 444:267–269.

Nemmar A, Hoylaerts MF, Hoet PH, Dinsdale D, Smith T, Xu H, Vermylen J, and Nemery B. 2002. Ultrafine particles affect experimental thrombosis in an in vivo hamster model. Am J Respir Crit Care Med 166:998–1004.

Oberdörster G, Maynard A, Donaldson K, Castranova V, Fitzpatrick J, Ausman K, Carter J, Karn B, Kreyling W, Lai D, Olin S, Monteiro-Riviere N,

Warheit D, and Yang H. 2005a. Principles for characterizing the potential human health effects from exposure to nanomaterials: Elements of a screening strategy. Particle Fibre Toxicol 2:1–35.

Oberdörster G, Oberdörster E, and Oberdörster J. 2005b. Nanotoxicology: An emerging discipline evolving from studies of ultrafine particles. Environ Health Perspect 113:823–839.

Oberdörster G, Sharp Z, Atudorei V, Elder A, Gelein R, Lunts A, Kreyling W, and Cox C. 2002. Extrapulmonary translocation of ultrafine carbon particles following whole-body inhalation exposure of rats. J Toxicol Environ Health A 65:1531–1543.

Oeff K, and Konig A. 1955. [Blood volume of rat organs and residual amount of blood after blood letting or irrigation; determination with radiophosphorus-labeled erythrocytes.]. Naunyn Schmiedebergs Arch Exp Pathol Pharmakol 226:98–102.

Rinderknecht, A, Prud'homme, R, Poreda R Gelein R, Corson N, Pidruczny A, Finkelstein J, Oberdörster G, and Elder A. 2008. Biokinetics of AU nanoparticles relative to size surface coating and portal of entry. Presented at the 47th Annual Society of Toxicology Meeting, March 2008, Seattle WA. Toxicologist 102:abstr. 1404.

Roth C, Ferron GA, Karg E, Lentner B, Schumann G, Takenaka S, and Heyder J. 2004. Generation of ultrafine particles by spark discharging. Aerosol Sci Technol 38:228–235.

Semmler M, Seitz J, Erbe F, Mayer P, Heyder J, Oberdorster G, and Kreyling WG. 2004. Long-term clearance kinetics of inhaled ultrafine insoluble iridium particles from the rat lung, including transient translocation into secondary organs. Inhal Toxicol 16:453–459.

Semmler-Behnke M, Takenaka S, Fertsch S, Wenk A, Seitz J, Mayer P, Oberdorster G, and Kreyling WG. 2007. Efficient elimination of inhaled nanoparticles from the alveolar region: Evidence for interstitial uptake and subsequent reentrainment onto airways epithelium. Environ Health Perspect 115: 728–733.

Szymczak, W, Menzel, N, Kreyling, WG, and Wittmaack, K. 2006. TOF-SIMS characterisation of spark-generated nanoparticles made from pairs of Ir–Ir and Ir–C electrodes. Int J Mass Spectrom 254:70–84.